Journal of Applied Polymer Science

Electrospun nylon 6,6 nanofibers functionalized with cyclodextrins for removal of toluene vapor

Fatma Kayaci,[1,2] Huseyin Sener Sen,[2] Engin Durgun,[1,2] Tamer Uyar[1,2]
[1]Institute of Materials Science & Nanotechnology, Bilkent University, Ankara 06800, Turkey
[2]UNAM-National Nanotechnology Research Center, Bilkent University, Ankara 06800, Turkey
Correspondence to: T. Uyar (E-mail: tamer@unam.bilkent.edu.tr)

ABSTRACT: Functional nylon 6,6 nanofibers incorporating cyclodextrins (CD) were developed via electrospinning. Enhanced thermal stability of the nylon 6,6/CD nanofibers was observed due to interaction between CD and nylon 6,6. X-ray photoelectron spectroscopy and attenuated total reflectance Fourier transform infrared spectroscopy studies indicated the existence of some CD molecules on the surface of the nanofibers. Electrospun nylon 6,6 nanofibers without having CD were ineffective for entrapment of toluene vapor from the environment, whereas nylon 6,6/CD nanofibrous membranes can effectively entrap toluene vapor from the surrounding by taking advantage of the high surface-volume ratio of nanofibers with the added advantage of inclusion complexation capability of CD presenting on the nanofiber surface. The modeling studies for formation of inclusion complex between CD and toluene were also performed by using *ab initio* techniques. Our results suggest that nylon 6,6/CD nanofibrous membranes may have potential to be used as air filters for the removal of organic vapor waste from surroundings. © 2015 Wiley Periodicals, Inc. J. Appl. Polym. Sci. **2015**, *132*, 41941.

KEYWORDS: electrospinning; fibers; nanostructured polymers; properties and characterization

Received 8 July 2014; accepted 2 January 2015
DOI: 10.1002/app.41941

INTRODUCTION

Air pollution is undoubtedly a major threat to the human health as industrialization and world population are growing day by day.[1,2] In addition to aerosols, volatile organic compounds (VOC) into air are of the major pollutants daily inhaled, and can cause serious sicknesses such as fatigue, headache, and even cancer.[2–6] The entrapment of VOC from indoor and outdoor environments is a high importance necessity for a healthier life. More practical and more efficient VOC removal techniques are in demand, since use of several methods including physical, chemical, and biological treatments to remove VOC still have limitations and challenges to sudden loading stresses. Air filters can remove VOC by mostly adsorption.[5,7] The nanofibrous membranes obtained via electrospinning are desirable filtering materials due to their exclusive properties such as very high surface area to volume ratio, nanoporous structure, high permeability, low basis weight.[7–15] Moreover, during electrospinning or post-processing, design flexibility of the nanofibers with chemical/physical functionalization may promote their applicability in filtration.[16–22]

Cyclodextrins (CD) that are cyclic oligosaccharides consisting of α(1,4)-linked glucopyranose units with a toroid-shaped molecular structure are extensively used in separations, purification, and filtration purposes due to their unique property to form inclusion complexes (IC) with hazardous and polluting organic compounds.[23–28] Therefore, the hydrophobic cavity of CD acts as a host for various organic guest molecules.[29–31] There are several types of non-covalent binding forces such as van der Waals interactions, hydrogen bonding between host CD and guest molecules. The most common CD types having six, seven, and eight glucopyranose units are named as α-CD, β-CD, and γ-CD, respectively.[29,30] While the height of the CD cavity is the same (∼8 Å) for all three types, the number of glucopyranose units determine the internal diameter of the cavity as ∼6 Å, 8 Å, and 10 Å for α-CD, β-CD, and γ-CD, respectively [Figure 1(a)].[29,30] The formation and stability of the CD-IC depend on many factors such as size/shape match and binding forces between the CD host and guest molecules.[32,33]

Our particular interest is the functionalization of electrospun nanofibrous membranes with CD that can provide efficient entrapment of organic waste compounds from the surroundings by combining the IC formation capability of CD with the adsorption capability of very high surface area of the nanofibers.[21,22,34–37] In our recent studies, we reported that nanofibers incorporating CD can remove organic waste molecules from

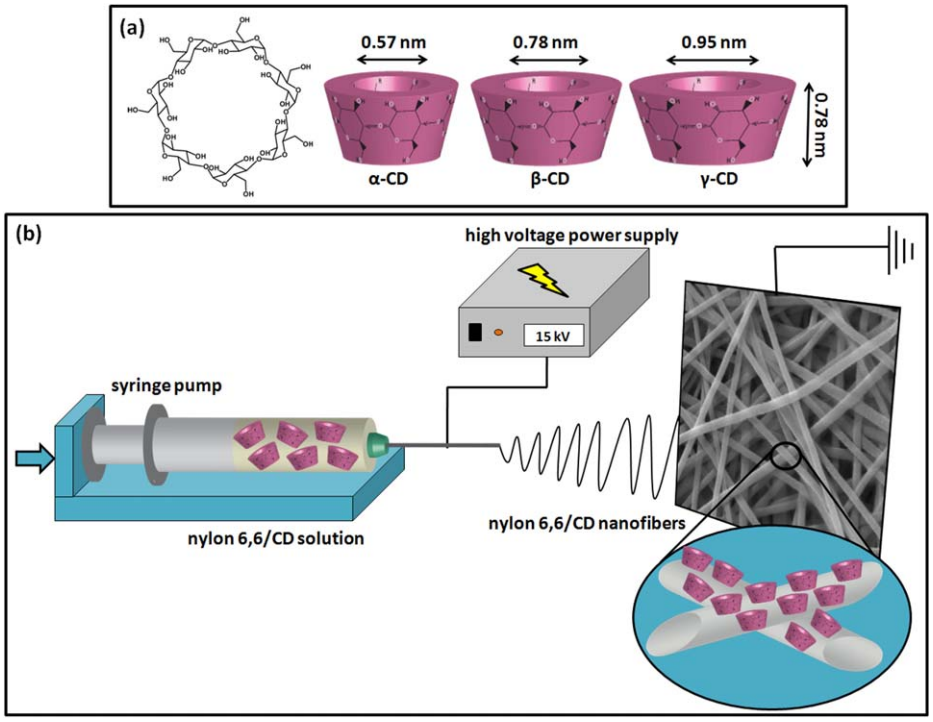

Figure 1. Schematic representations of (a) chemical structure of β-CD and approximate dimensions of α-CD, β-CD, γ-CD, and (b) electrospinning of nylon 6,6/CD solution. [Color figure can be viewed in the online issue, which is available at wileyonlinelibrary.com.]

vapor phase[34,35] and liquid media.[21,22,36,37] Physically bounded CD onto nanofibers could leach out from the nanofiber matrix in aqueous medium, since CD are water soluble. Therefore, CD-functionalized nanofibers are more useful for removal of VOC without any leaching problem.

Here, our aim was to remove of VOC from environment by using the CD functionalized nanofibrous membranes and investigate the effect of not only CD amount, but also type of CD on the entrapment efficiency of VOC. Moreover, in this study, we have investigated not only experimental but also theoretical results to evaluate the effect of CD type on the trapping efficiency of VOC. With this purpose, we have produced the CD functionalized electrospun nylon 6,6 nanofibers (nylon 6,6/CD) by using α-CD, β-CD, and γ-CD in two different % weight loading (25% and 50%, w/w, with respect to nylon 6,6). Figure 1(b) indicates the schematic representation of the electrospinning of nylon 6,6/CD solution. Electrospun nylon 6,6 nanofibrous membranes have been indicated as a suitable material for filtration application in the literature,[38–40] which is the reason of the selection of the nylon 6,6 as a nanofibrous polymeric matrix in this study. The morphological, structural, thermal, and surface characteristics of the nylon 6,6 and nylon 6,6/CD nanofibers were investigated. Thereafter, toluene that is widely used as an industrial feedstock and a solvent was used as a model of VOC. The removing of toluene vapor from environment is of quite importance, since inhalation of toluene can cause tiredness, confusion, weakness, memory loss, nausea, loss of appetite, hearing and color vision loss, unconsciousness, and even death. Toluene vapor entrapment capability of nylon 6,6 and nylon 6,6/CD nanofibrous membranes was tested. We have also performed the modeling studies for formation of IC between toluene and CD (α-CD, β-CD, and γ-CD) by using *ab initio* techniques. Based on the obtained results, nylon 6,6/CD nanofibrous membranes could be considered as a suitable candidate for removal of VOC from out/indoor environments.

EXPERIMENTAL

Materials

Three types of native CD (α-CD, β-CD, and γ-CD) were purchased from Wacker Chemie AG. Nylon 6,6 pellets (relative viscosity: 230.000–280.000), formic acid (98–100%), toluene (puriss., $\geq$99.5%), and acetonitrile chromasolv (99.9%) were purchased from Sigma-Aldrich. All chemicals were used as-received without any further purification.

Preparation of the Solutions for Electrospinning

Nylon 6,6 solution without CD was prepared by dissolving 10% (w/v) nylon 6,6 in formic acid. In the case of nylon 6,6/CD solutions, α-CD, β-CD, and γ-CD in different ratio (25% and 50%, w/w, with respect to nylon 6,6) were dissolved in formic acid and then, nylon 6,6 (10%, w/v) was added to each CD solution individually and stirred for 3 h at room temperature to obtain homogeneous and clear solutions. Table I summarizes the compositions of the resulting nylon 6,6 and nylon 6,6/CD solutions used for electrospinning.

Electrospinning

The individual nylon 6,6 and nylon 6,6/CD solutions were loaded into 10 mL syringes fitted with metallic needles (~0.7 mm inner diameter). The syringes were placed horizontally on the syringe pump (KDS 101, KD Scientific). The feed

Table I. Properties of Nylon 6,6 and Nylon 6,6/CD Solutions and the Resulting Nanofibers

Samples	% Nylon (w/v)[a]	Type of CD, % (w/w)[b]	Viscosity (Pa s)	AFD (nm)	Fiber morphology
Nylon 6,6	10	–	0.063	95 ± 15	Bead-free nanofibers
Nylon 6,6/25α-CD	10	α-CD, 25	0.078	105 ± 20	Bead-free nanofibers
Nylon 6,6/25β-CD	10	β-CD, 25	0.072	110 ± 25	Bead-free nanofibers
Nylon 6,6/25γ-CD	10	γ-CD, 25	0.084	110 ± 20	Bead-free nanofibers
Nylon 6,6/50α-CD	10	α-CD, 50	0.113	140 ± 35	Bead-free nanofibers
Nylon 6,6/50β-CD	10	β-CD, 50	0.097	130 ± 25	Bead-free nanofibers
Nylon 6,6/50γ-CD	10	γ-CD, 50	0.106	130 ± 20	Bead-free nanofibers

[a] With respect to solvent (formic acid).
[b] With respect to polymer (nylon).

rate of the solutions was set to 1 mL/h during electrospinning. The high voltage power supply (Matsusada, AU Series) was used to apply a voltage of +15 kV for the electrospinning. Randomly oriented nanofibers were deposited on a grounded stationary cylindrical metal collector (height: 15 cm, diameter: 9 cm) covered by a piece of aluminum foil and located at 10 cm from the end of the tip. The electrospinning process was performed at ~23°C and 29% relative humidity in an enclosed Plexiglas chamber.

Measurements and Characterizations

Anton Paar Physica MCR 301 Rheometer equipped with cone/plate accessory (spindle type CP40-2) was used to measure the viscosity of the each solution used for electrospinning at 22°C and a constant shear rate of 100 s^{-1}. Scanning electron microscope (SEM, FEI-Quanta 200 FEG) was employed to investigate the morphology and dimensions of nylon 6,6 and nylon 6,6/CD nanofibers. A nominal 5 nm Au/Pd was sputtered on the samples prior to SEM analysis. The average fiber diameters (AFD) of the samples were determined taking about 100 measurements from the SEM images of each sample. X-ray diffraction (XRD) patterns of the nanofibers were recorded in the range of $2\theta = 5°–30°$ using PANalytical X'Pert Pro Multi Purpose X-ray diffractometer with Cu Kα radiation ($\lambda = 1.5418$ Å). Thermogravimetric analyzer (TGA, TA Q500) was used to investigate the thermal properties of the nanofibers. TGA measurements were performed from room temperature to 600°C at a constant heating rate of 20°C/min under the nitrogen atmosphere. The surface chemical characterizations of the nanofibers were performed by attenuated total reflectance Fourier transform infrared spectroscopy (ATR-FTIR, Bruker, VERTEX 70) and X-ray photoelectron spectroscopy (XPS, Thermo Scientific K-Alpha, monochromated Al Kα X-ray source, $hv = 1486.6$ eV) with flood gun charge neutralizer. The ATR-FTIR spectra were recorded with FTIR spectrometer equipped with ATR set up containing a germanium crystal and a liquid nitrogen-cooled mercury cadmium telluride detector. Each spectrum over a range 900–3700 cm^{-1} was obtained with a resolution of 4 cm^{-1} by taking 64 scans. XPS wide energy survey scans (0–1360 eV) and the O 1s core-level spectra were obtained from the surface of the samples (400 μm spot size) at pass energy of 150 and 50 eV with energy step size of 1 and 0.1 eV, respectively. Peak deconvolutions for the core-level spectra were performed with Avantage software.

Entrapment of Toluene Vapor by the Nanofibrous Membranes

Toluene was used as a model VOC in order to investigate the molecular entrapment capability of the nylon 6,6, nylon 6,6/25α-CD, nylon 6,6/25β-CD, nylon 6,6/25γ-CD, nylon 6,6/50α-CD, nylon 6,6/50β-CD, and nylon 6,6/50γ-CD nanofibers. The nanofibrous membranes were exposed to the toluene vapor in a sealed glass desiccator (30 cm [diameter] and 30 cm [height]) at ~24°C and 30% relative humidity. In this experiment, a glass Petri dish including 20 mL of toluene (as-received, without any dilution) was located at the bottom of desiccator while three pieces of each sample (about 22 mg, 4 × 4 cm^2) were placed on the supporting layer positioned at 7 cm high from the bottom of desiccator. After the electrospun nanofibrous membranes were kept in this sealed desiccator for 12 h to expose to excess toluene vapor, they were taken out of the desiccator and kept in the suction hood for 5 h in order to remove the uncomplexed toluene molecules that were only adsorbed on the membranes. Finally, high performance liquid chromatography (HPLC, Agilent 1200 series) equipped with VWD UV detector was used in order to determine the amount of toluene entrapped by the membranes. For this, each membrane was immersed in 4 mL ACN and kept in it for 2 h to extract toluene from the membranes. Then 0.5 mL of these solutions was put into HPLC vials, individually to measure toluene concentration in them. Injection volume was set to 5 μL and toluene was detected at 254 nm, in 4 min using the Agilent C18 column (150 × 4.6 mm^2, 5 μm pores) and ACN (100%) as a mobile phase with the 0.5 mL/min of flow rate. The toluene peak areas in the resulting HPLC chromatograms were converted to toluene concentration using the calibration curve ($R^2 = 0.999$) that was prepared using toluene solutions having different concentrations (58, 29, 14.5, 7.2, 3.6, 1.8, and 0.9 ppm).

Computational Method

The structures of toluene, α-,[41,42] β-,[43] and γ-CD,[44] and their ICs were optimized by using *ab initio* methods based on density functional theory,[45,46] implemented in the Vienna *ab initio* simulation package.[47,48] The initial geometries were obtained from Cambridge Structural Database.[49] The exchange-correlation was

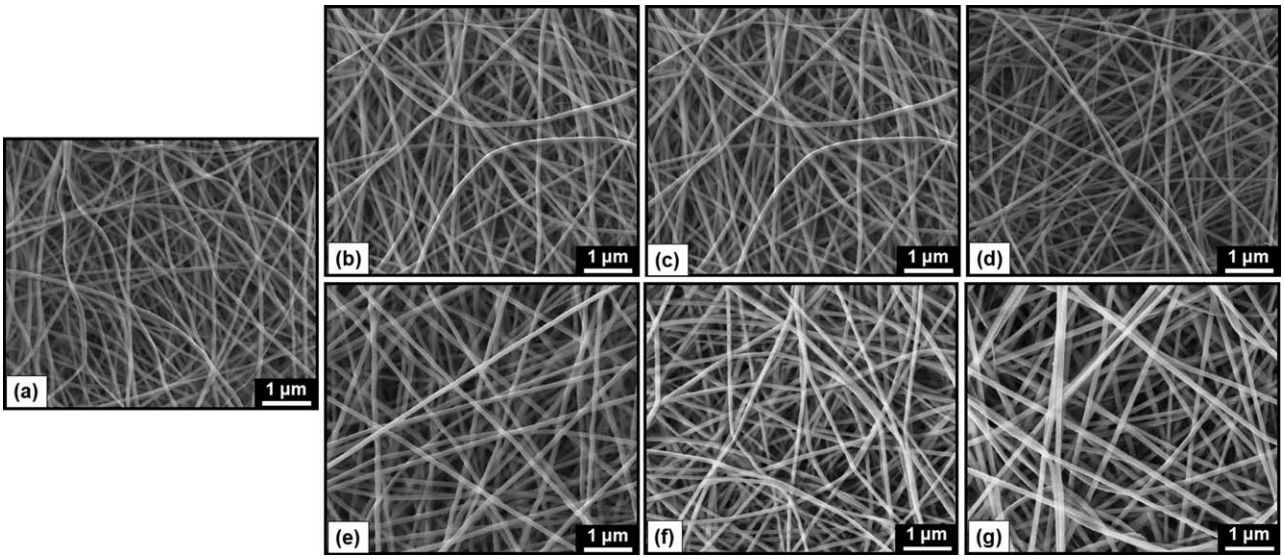

Figure 2. Representative SEM images of electrospun nanofibers from the solutions of (a) nylon 6,6, (b) nylon 6,6/25α-CD, (c) nylon 6,6/25β-CD, (d) nylon 6,6/25γ-CD, (e) nylon 6,6/50α-CD, (f) nylon 6,6/50β-CD, and (g) nylon 6,6/50γ-CD.

treated within Perdew-Burke-Enzerhof of parameterization of the generalized gradient approximation[50] with inclusion of Van der Waals correction.[51] The element potentials were described by projector augmented-wave method[52] using a plane-wave basis set with a kinetic energy cutoff of 400 eV. The Brillouin zone integration was performed at the gamma-point. All structures were considered as isolated molecules in a vacuum and were relaxed using the Kosugi algorithm with simultaneous minimization of the total energy and interatomic forces. The convergence on the total energy and force was set to 10^{-5} eV and 10^{-2} eV/Å, respectively.

RESULTS AND DISCUSSION

Morphological Characterization of the Nanofibers

The representative SEM images of nylon 6,6 and nylon 6,6/CD nanofibers are given in Figure 2. Bead-free nanofibers were yielded from the nylon 6,6 (10%, w/v) solutions both without and with CD. The properties of the solutions (composition and viscosity) and the resulting electrospun nanofibers (AFD and morphology) are summarized in Table I. It was observed that the AFD of nylon 6,6/CD nanofibers was slightly increased when compared to pristine nylon 6,6 nanofibers. This is possibly due to greater resistance to stretching and elongation of the electrified jet of nylon 6,6/CD solutions having higher solution viscosity, and that is comparable with the general observation in the literature.[53–55] Moreover, as the content of the CD increased from 25% to 50% (w/w, with respect to nylon 6,6) viscosity of the solutions increased too, and larger AFD was yielded for the nylon 6,6/50CD. A possible reason for the viscosity increase may be some interaction (H bonds) between the CD molecules and nylon 6,6 polymer chains, which is given in ATR-FTIR discussion later on.[56]

Structural Characterization of the Nanofibers

In order to investigate whether any crystalline CD aggregates were present in the fiber matrix or not, XRD patterns of the as-received CD and nanofibers were obtained (Figure 3). The as-received α-CD, β-CD and γ-CD have "cage type" crystalline structures in which cavity of each CD molecule is blocked by the adjacent CD molecules,[55,57] and so their XRD patterns have distinct diffraction peaks that are annotated in Figure 3(a): $2\theta \cong 12.0°$, 14.4°, 21.7° for α-CD, $2\theta \cong 10.8°$, 12.6°, 19.7°, 21.3° for β-CD and $2\theta \cong 12.3°$, 16.5°, 21.8° for γ-CD. However, the broad halo XRD patterns of pristine nylon 6,6 and nylon 6,6/CD electrospun nanofibrous membranes [Figure 3(b)] did not show any crystalline peaks of α-CD, β-CD, and γ-CD, indicating that all three types of CD were distributed in the nylon 6,6 fiber matrix without forming crystal aggregates. Compared to CD powder having cage type crystalline structure, cavities of CD dispersed within the fiber matrix are more available for complexation with the aromatic molecules from the environment. On the other hand, it is known that nanofibers including CD have very large surface area compared to CD powder. Therefore, the combination of the very high surface area of electrospun nanofibers with the higher inclusion complexation capability of CD molecules increases the VOC entrapment efficiency.

In Figure 3(b), the XRD pattern of pure nylon 6,6 nanofibers exhibited the reflection of (100) and (010, 110) planes at about 20.3° and 23.7° indicating α-type crystals structure of nylon 6,6 (triclinic phase).[58–61] The α1 peak ($2\theta \cong 20.3°$) arises from the distance between hydrogen bonded chains, while the separation of hydrogen-bonded planar sheets results in the occurrence of α2 peak ($2\theta \cong 23.7°$).[58,59,62,63] As stated in the literature, besides α phase, γ phase showing peaks at about 13.33° and 22.2° can also exist in nylon 6,6. However, γ phase illustrating pleated sheets of methylene units with hydrogen bonding between sheets rather than within sheets, is more thermodynamically unstable than α phase, and so it does not often appear in nylon 6,6 at room temperature.[63,64] The XRD patterns of all nylon 6,6/CD nanofibers are very similar to the XRD pattern of pure nylon 6,6 nanofibers as displayed Figure 3(b), indicating the crystalline structure of nylon 6,6 (only α phase/triclinic) have remained unchanged with the presence of CD.

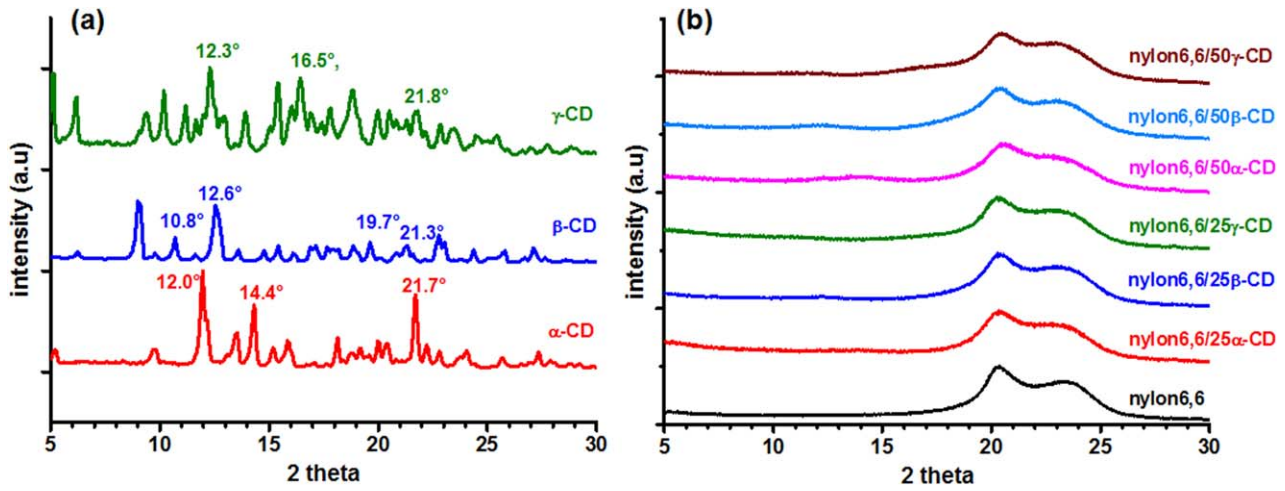

Figure 3. XRD patterns of (a) as-received CD and (b) the electrospun nanofibers. [Color figure can be viewed in the online issue, which is available at wileyonlinelibrary.com.]

On the other hand, the inclusion complexation possibility between nylon chains and CD has been reported in the literature under specific conditions (heating technique) and certain solution preparation procedure.[65–67] In those studies, the precipitation of the IC occurred in the prepared solutions and the characteristic XRD peaks of "channel-type" CD crystal structure in which CD molecules are aligned and stacked on top of each other,[56,57,68] were confirmed the inclusion complexation between CD and nylon.[65–67] However, we did not observe neither precipitation nor channel-type CD crystal structure in our XRD results suggested that CD and nylon 6,6 chains did not form IC in our experimental conditions. It is known that the IC formation between host molecules and guest CD is affected by process temperature, solvent type, and host/guest ratio.[29]

Thermal Characterization of the Nanofibers

TGA was used to investigate thermal characteristics of the samples and to determine the weight percentage of CD in the resulting electrospun nylon 6,6/CD nanofibers. We found out that TGA data of nylon 6,6/CD nanofibers obtained from α-CD, *β*-CD, and *γ*-CD were almost same. So as a representative data, TGA and derivative of TGA thermograms of nylon 6,6/α-CD nanofibers (nylon 6,6/25α-CD, nylon 6,6/50α-CD) compared with pristine nylon 6,6 nanofibers and α-CD are only given in Figure 4.

The TGA of pure α-CD has an initial weight loss (∼10%) below 100°C and major weight loss between 275 and 365°C owing to water loss and main degradation of CD, respectively.[69,70] The degradation of nylon 6,6 nanofibers occurs between 345 and 490°C as it is seen in the TGA thermogram of pristine nylon 6,6 nanofibers. The observation of CD degradations in the TGA thermograms of nylon 6,6/CD nanofibers confirmed the incorporation of CD molecules in the nylon 6,6 fiber matrix. It is obvious from these thermograms that the thermal stability of CD within nanofibers is higher than that of as-received CD. Therefore, the degradation of α-CD was observed in the range of 290–390°C and 290–400°C for nylon 6,6/25α-CD and nylon 6,6/50α-CD nanofibers, respectively. The degradations of *β*-CD and *γ*-CD in the nanofibers also started at ∼290°C, however, they carried out until approximately 385 and 375°C for nylon 6,6/25*β*-CD and nylon 6,6/25*γ*-CD, respectively; 395 and 390°C for nylon 6,6/50*β*-CD and nylon 6,6/50*γ*-CD, respectively (data not shown). The increase of degradation

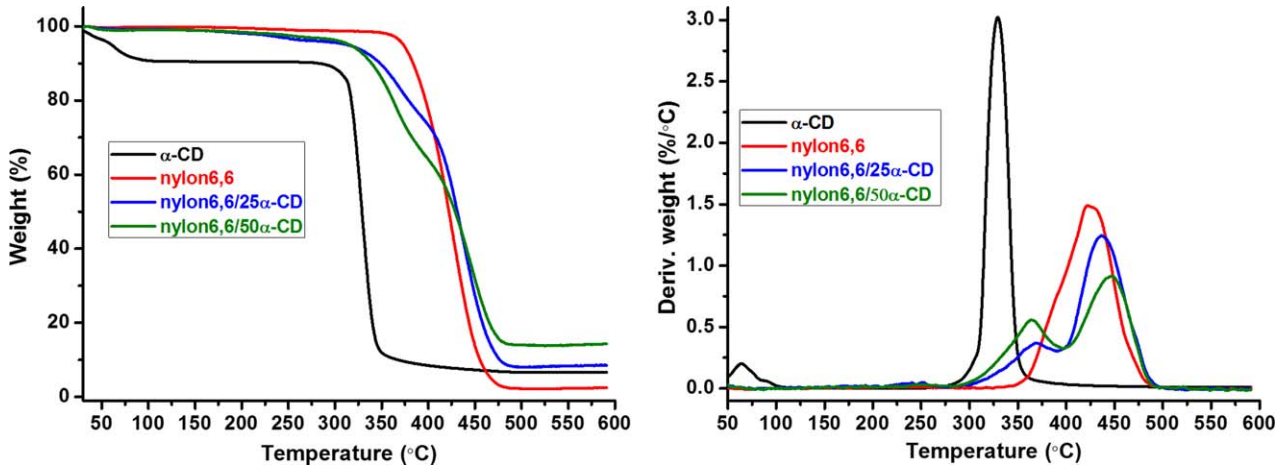

Figure 4. TGA and derivative TGA thermograms of as-received α-CD and the electrospun nanofibers. [Color figure can be viewed in the online issue, which is available at wileyonlinelibrary.com.]

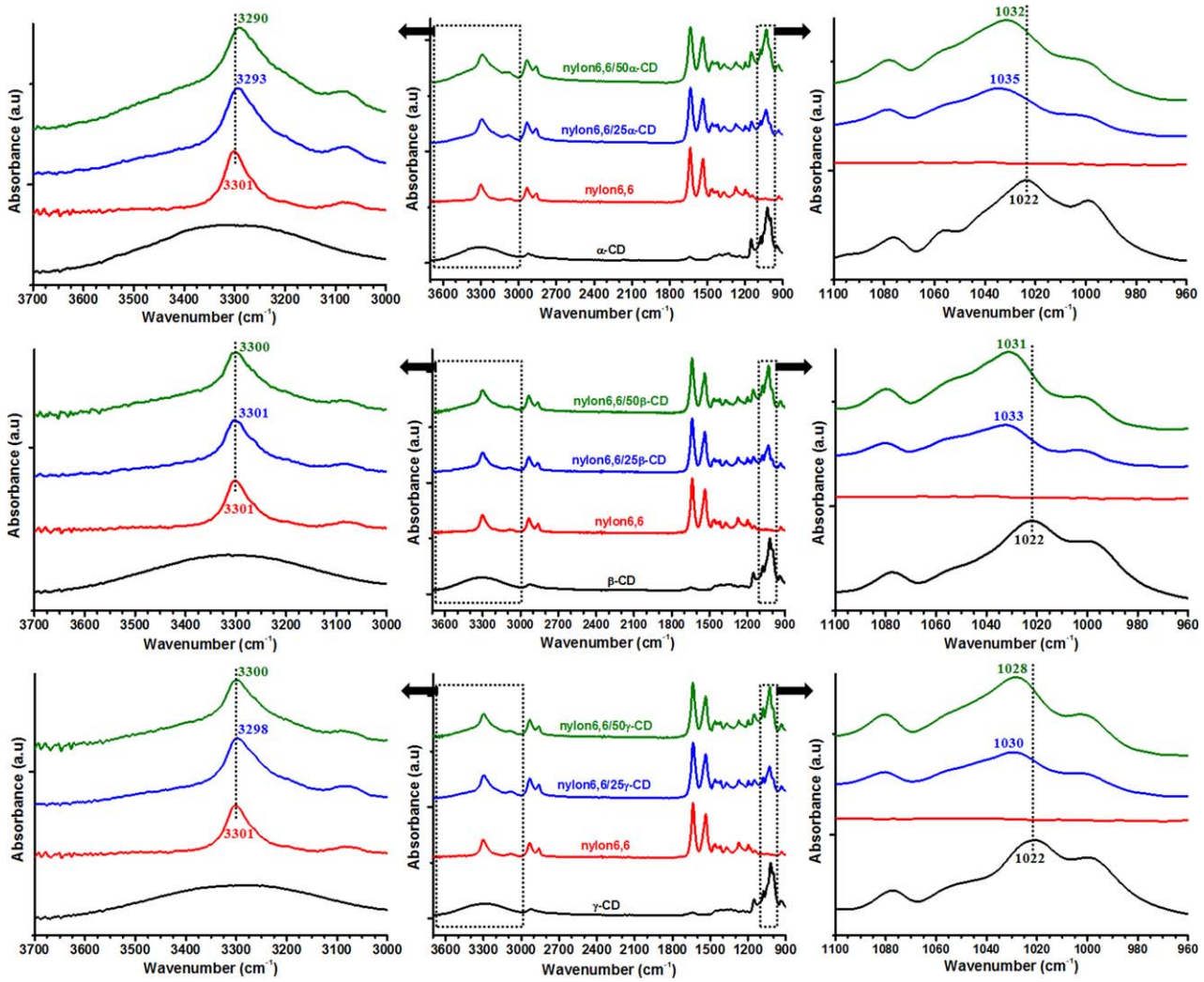

Figure 5. ATR-FTIR spectra of the as received CD, electrospun nylon 6,6 and nylon 6,6/CD nanofibers. Enlarged region of these spectra are given at left side (between 3700 and 3000 cm^{-1}) and right side (between 1100 and 960 cm^{-1}). [Color figure can be viewed in the online issue, which is available at wileyonlinelibrary.com.]

temperature of CD in the nanofibers occurred depending on CD type and amount in the nanofibers. Moreover, we also observed that the thermal degradation of nylon 6,6 in the nylon 6,6/CD nanofibers was also shifted to slightly higher temperature with increasing CD content. The improved thermal stability of the resulting nylon 6,6/CD nanofibers are attributed to the interaction between the polymeric matrix and the CD which is verified by the ATR-FTIR data. The increase of thermal stability of CD in electrospun nylon 6,6-CD nanofibers can be further improved the applicability of these nanofibers.

The amount of CD present in the nylon 6,6/CD nanofibers was calculated from TGA thermograms as approximately 18% and 33% weight in nylon 6,6/25α-CD and nylon 6,6/50α-CD nanofibers, respectively. About 17% and 33% weight β-CD were determined in nylon 6,6/25β-CD and nylon 6,6/50β-CD nanofibers, respectively. In the case of nylon 6,6/25γ-CD and nylon 6,6/50γ-CD nanofibers, γ-CD was calculated as nearly 19% and 35%, respectively. In order to prepare nylon 6,6/25CD and nylon 6,6/50CD solutions 20% and 40% (w/w, with respect to sample) CD hydrates including about 10% water were used, respectively. The actual initial content of CD in nylon 6,6/CD solutions were calculated as ~18% and ~36% (w/w, with respect to sample) by

Table II. Atomic Concentrations Generated from XPS Wide Energy Survey Scans

Samples	C (%)	O (%)	N (%)
α-CD	58.45	41.55	-
β-CD	57.69	42.31	-
γ-CD	58.47	41.53	-
Nylon 6,6	75.45	12.67	11.88
Nylon 6,6/25α-CD	74.25	14.87	10.88
Nylon 6,6/25β-CD	75.86	14.43	9.71
Nylon 6,6/25γ-CD	74.65	14.13	11.22
Nylon 6,6/50α-CD	74.28	17.05	8.67
Nylon 6,6/50β-CD	69.35	20.25	10.4
Nylon 6,6/50γ-CD	74.58	18.37	7.05

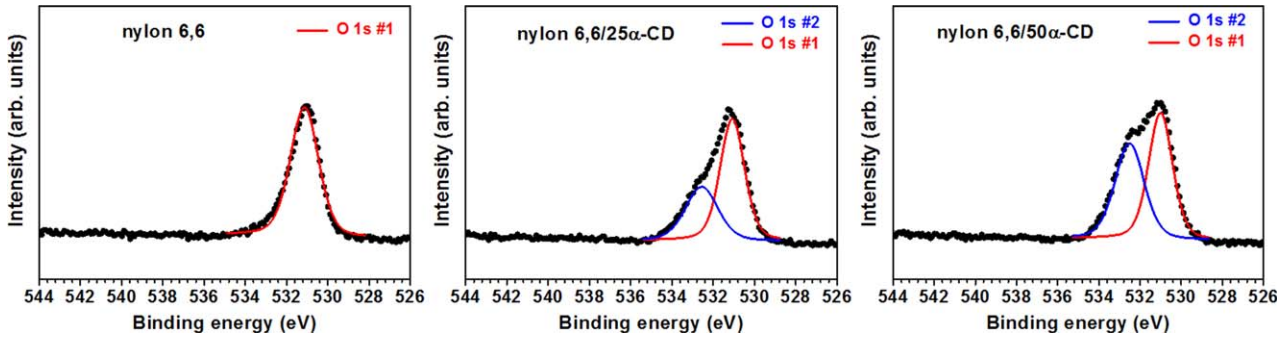

Figure 6. Core-level XPS spectra of O 1s from the nanofibers. [Color figure can be viewed in the online issue, which is available at wileyonlinelibrary.com.]

subtracting the water amount. As a result, the calculation for nylon 6,6/25CD nanofibers almost matched with the initial amount of CD added in nylon 6,6/25CD solutions. In addition, the γ-CD content in nylon 6,6/50γ-CD nanofibers was also coherent with the initial amount in that solution. However, the CD amount was calculated slightly less amount for nylon 6,6/50α-CD and nylon 6,6/50β-CD nanofibers possibly because of overlapping of degradation temperatures of nylon 6,6 and CD. On the other hand, we did not observe any weight loss up to 100°C in the TGA thermograms of nylon 6,6/CD nanofibers despite of 10% water in pure CD, indicating the cavities of CD in the nanofibers are free of water, similar to our previous studies.[34,56]

Surface Chemical Characterization of the Nanowebs

Phase separation of CD from polymer matrix is quite possible during solvent evaporation in the electrospinning process due to their different hydrophilic/hydrophobic nature, and certain amount of CD molecules may reside on the polymeric fiber surface.[34,36,37,71] To confirm the presence of CD on the surface of the nylon 6,6/CD nanofibers that is quite important for entrapment efficiency of VOC,[34,35] surface chemical characterization of the nanowebs were performed by using ATR-FTIR and XPS techniques.

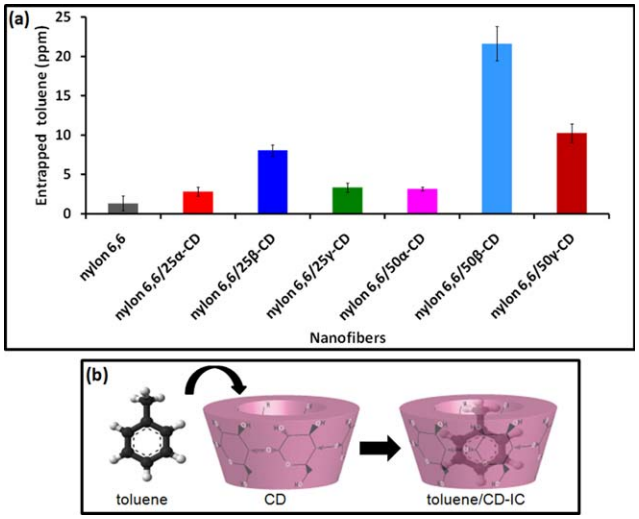

Figure 7. (a) The amount of entrapped toluene (ppm) by the electrospun nanofibers and (b) schematic representation of the formation of toluene/CD-IC. [Color figure can be viewed in the online issue, which is available at wileyonlinelibrary.com.]

The ATR-FTIR spectra in the region from 3700 to 900 cm^{-1} obtained for the as-received CD, electrospun nylon 6,6 and nylon 6,6/CD nanofibers are shown in Figure 5. The spectrum of pristine nylon 6,6 nanofibers exhibited main characteristic peaks at 3301 cm^{-1} (N—H stretching vibration), 2934 cm^{-1} (—CH_2 stretching vibration), 2860 cm^{-1} (—CH— symmetric stretching vibration), 1637 cm^{-1} (—C═O stretching vibration) and 1536 cm^{-1} (N—H bending vibration).[61,72] These peaks were also observed in the spectra of nylon 6,6/CD nanofibers. On the other hand, the ATR-FTIR spectra of the semicrystalline nylon 6,6 and nylon 6,6/CD nanofibers have α-type crystalline phase located at 934, 1199, and 1475 cm^{-1} and amorphous components indicated at 1141 and 1180 cm^{-1}.[60,72] The absence of the FTIR peak at 977 cm^{-1} assigned to the γ-type crystalline phase[64,66] in the spectra of the nanofibers confirmed that the CD did not change the crystalline structure of nylon 6,6, which is coherent with the XRD data.

In the ATR-FTIR spectra of α-CD, β-CD, and γ-CD (Figure 5), the very broad band between 3000 and 3700 cm^{-1} assigned to the symmetric and antisymmetric O—H stretching vibrations and the absorption peak at about 2924 cm^{-1} corresponding to C—H bond of CD was observed.[73,74] The obvious characteristic CD peaks at between 1000 and 1100 cm^{-1} attributed to coupled C—C/C—O stretching vibrations, and the peak at 1152 cm^{-1} assigned to the antisymmetric stretching vibration of the C—O—C glycosidic bridge[34,56,69,71,75] were identified in all ATR-FTIR spectra of nylon 6,6/CD nanofibers, but not in the spectrum of pristine nylon 6,6 nanofibers. The enhanced intensity of these CD related peaks was also clearly observed as the CD content increased from 25% through 50% (w/w) in the nylon 6,6/CD nanofibers. This result indicated the existence of CD on the surface of the nylon 6,6/CD nanofibers, and the inclusion complexation capability of these CD could be used for the removal of VOC from the environment.

Moreover, it was observed in the enlarged region of ATR-FTIR spectra between 3700 and 3000 cm^{-1} (Figure 5, left side) that the N—H stretching peak of nylon 6,6 was generally shifted to lower wavenumber for nylon 6,6/CD nanofibers when compared to pure nylon 6,6 nanofibers. On the other hand, the enlarged region of FTIR spectra between 1100 and 960 cm^{-1} in Figure 5, right side indicated the obvious CD peak shift to higher

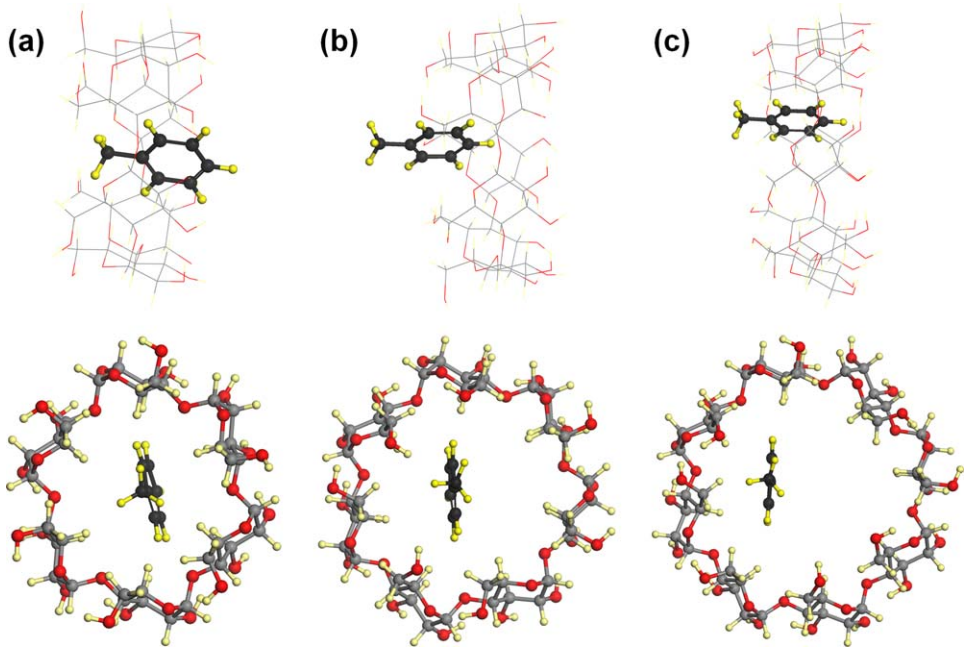

Figure 8. Side and top view of optimized structures of single toluene and (a) α-, (b) β-, (c) γ-CD IC (1 : 1). Gray, red, and yellow spheres represent carbon, oxygen, and hydrogen atoms, respectively. [Color figure can be viewed in the online issue, which is available at wileyonlinelibrary.com.]

wavenumber for nylon 6,6/CD nanofibers compared to pure CD. The shifts of these FTIR peaks for nylon 6,6/CD nanofibers possibly due to hydrogen bonding between nylon 6,6 and CD. More distinctive peak shifts were observed for nylon 6,6/α-CD nanofibers possibly due to smaller size of α-CD which can more interact with the nylon 6,6 chains. The higher thermal degradation temperature of α-CD in the nanofibers compared to other CD types, which discussed in TGA discussion is possibly because of higher interaction between α-CD and nylon 6,6 chains. Similar FTIR peak shifts were also observed in our previous studies for zein/CD[69] and polyester (PET)/CD[34] nanofibers due to interaction between zein and CD, PET and CD.

In order to determine the CD amount on the surface of nylon 6,6/CD nanofibers, XPS technique was used providing more surface sensitivity compared to ATR-FTIR (i.e., about 10 nm depth for XPS and 650 nm depth for ATR-FTIR having germanium crystal, respectively).[71] The atomic concentrations of as-received CD and the electrospun nanofibers obtained from wide energy XPS survey spectra are indicated in Table II. The appearance of a

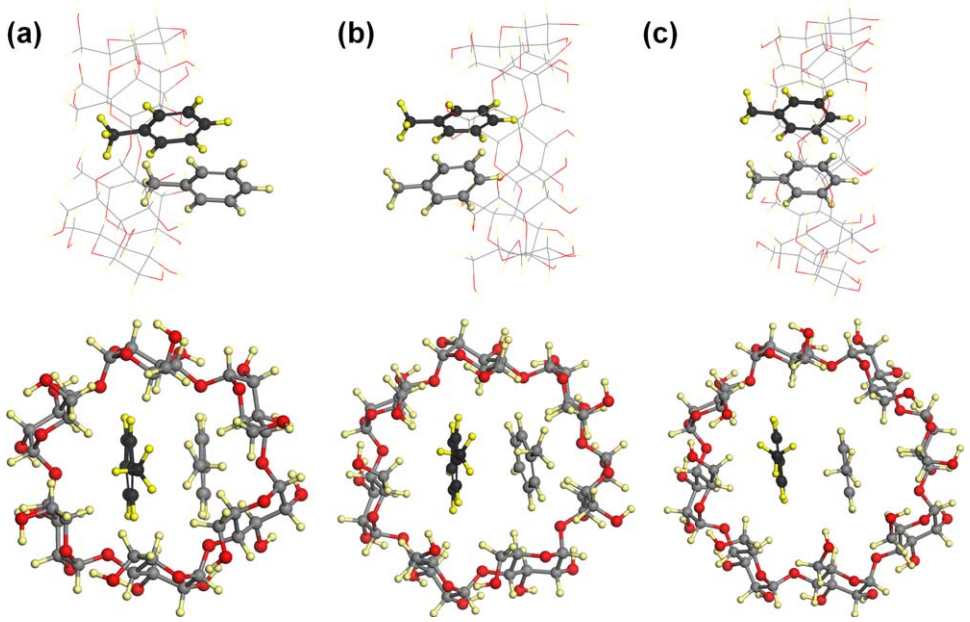

Figure 9. Side and top view of optimized structures of two toluene molecules and (a) α-, (b) β-, (c) γ-CD IC (2 : 1). Gray, red, and yellow spheres represent carbon, oxygen, and hydrogen atoms, respectively. [Color figure can be viewed in the online issue, which is available at wileyonlinelibrary.com.]

higher oxygen content outer surface of the nylon 6,6/CD nanofibers compared to pristine nanofibers provides evidence of the presence of CD on the fiber surface. Moreover, an increase in the surface oxygen content was also observed with the increasing amount of CD (from 25 to 50% [w/w]).

Furthermore, high energy resolution O 1s spectra of the nanofibers were also recorded to get more detailed information about the surface components and confirm the existence of CD onto surface of nylon 6,6/CD nanofibers. O 1s XPS spectra of pristine nylon 6,6, nylon 6,6/25α-CD and nylon 6,6/50α-CD nanofibers are given in Figure 6. Similar XPS spectra were also recorded for samples of nylon 6,6 nanofibers incorporating β-CD and γ-CD.

The spectrum of nylon 6,6 nanofibers has only π-bonded oxygen (C═O*) at peak binding energy of 531.13 eV.[76] On the other hand, beside this carbonyl group (O 1s #1) assigned to nylon 6,6 matrix, one more fitting peak (O 1s #2) was also represented at peak binding energy of about 532.53 in the nylon 6,6/CD spectra due to σ-bonded oxygen (C—O*C) and hydroxyl groups (C—O*H) of CD.[34,76] The higher ratio of O 1s #2 peak corresponding CD components was observed in nylon 6,6/50α-CD nanofibers compared to nylon 6,6/25α-CD sample. These results indicated that enhanced oxygen content on the surface of the nylon 6,6/CD nanofibers originated from the ether and alcohol groups of CD. Using the atomic concentrations obtained from XPS survey spectra (Table II), it was calculated that 8%, 6%, 5%, 15%, 26%, and 20% CD were present in the probed volume of nylon 6,6/25α-CD, nylon 6,6/25β-CD, nylon 6,6/25γ-CD, nylon 6,6/50α-CD, nylon 6,6/50β-CD, and nylon 6,6/50γ-CD nanofibers, respectively. It is known that the component having lower molecular weight in such blend systems generally migrates to the surface due to energetic and entropic effects.[34,77–80] Here, the lower concentrations of CD on the surface of the nylon 6,6/CD nanofibers compared to the compositions of the electrospun solutions indicated that some of the CD molecules situated on the fiber surface whereas some CD molecules were hidden in the bulk of the fiber matrix.

The Entrapment Efficiency of Toluene Vapor by Nanofibrous Membranes

Here, toluene vapor is selected as a model VOC since CD can form IC with toluene that is commonly used in industry for certain purposes.[26,81–83] The toluene vapor entrapment performance of the nylon 6,6 and nylon 6,6/CD nanofibers was compared. The amount of toluene entrapped by nanofibers was calculated by performing HPLC analyses and the data is given in Figure 7(a). Quite low amount of toluene (~1.3 ppm) was absorbed by pristine nylon 6,6 nanofibers most probably due to a very weak interaction between toluene and nylon 6,6 nanofibers. This suggest that nylon 6,6 nanofibrous membrane without CD has minimal capability of trapping toluene vapor.[35] In the case of nylon 6,6/CD nanofibers, the amount of entrapped toluene was considerable higher (at least two times) possible due to the complexation capability of the CD presenting on the nanofiber surface. The complex formation of toluene with CD cavity is illustrated in Figure 7(b), schematically.

Nylon 6,6/25α-CD, nylon 6,6/25β-CD, and nylon 6,6/25γ-CD nanofibers captured ~2.8, 8.1, and 3.4 ppm toluene, while the amount of toluene entrapped by nylon 6,6/50α-CD, nylon 6,6/50β-CD, and nylon 6,6/50γ-CD nanofibers was ~3.2, 21.6, 10.2 ppm. For each CD type, we observed that the amount of toluene entrapped was increased as the loading of CD in the nanofibers was increased from 25 to 50%, since the amount of CD existing on the fiber surface was also increased as confirmed by XPS data. When the CD types were compared, the amount of entrapped toluene vapor was on the order of nylon 6,6/β-CD > nylon 6,6/γ-CD > nylon 6,6/α-CD, indicating that the used CD type was quite important for the inclusion complexation owing to different size/shape match between the host CD and toluene. The IC formation depends on the relative size of the CD cavity to the size of the guest molecule.[36,70,84–86] Based on the different CD dimensions [Figure 1(a)], generally, α-CD can form complex for compounds with aliphatic side chains or low molecular weight molecules, β-CD can form complex with heterocycles and aromatics, and γ-CD can accommodate larger molecules such as steroids and macrocycles.[30,87] Therefore, each CD type can have different capability for the inclusion complexation with the same guest molecule. Our result indicated that β-CD cavity is more suitable host for toluene molecule possibly due to a better fit and size match between cavity size of β-CD and toluene molecule.[83] Moreover, nylon 6,6/50β-CD presented the highest toluene entrapment efficiency among the other samples, since the XPS survey scans shows that surface of this sample has highest amount of CD which could complex with more amount of toluene. It can be concluded that the toluene entrapping efficiency of the nanofibers depends on both the amount of surface associated CD molecules and the type of CD. In brief, the findings suggested that CD functionalized electrospun nylon 6,6 nanofibers would be very effective for the removal of VOC from the environment due to their very large surface area along with inclusion complexation capability of surface associated CD on the nanofibers.

Modeling Toluene Molecules Inside the CD Cavities

The stability of CD-IC when one (1 : 1) and two (2 : 1) toluene molecules included in CD is examined by using first-principles modeling techniques. First, the initial geometries of α-, β-, and γ-CD and toluene molecule(s) are fully optimized separately in vacuum. In order to form a complex, first single toluene molecule is introduced into each CD at various positions and with different orientations. For each case, the whole system is optimized without imposing any constraints. For the lowest energy configurations (Figure 8), the complexation energy (E_{comp}), which determines the stability of different complexes, is calculated as

$$E_{comp} = E_{CD} + n \times E_{toluene} - E_{toluene+CD}$$

where E_{CD}, $E_{toluene,}$ and $E_{toluene+CD}$ is the total energy (including van der Waals interaction) of CD (α, β, and γ), toluene, and toluene-CD complex, respectively, and n is the number of toluene molecules. E_{comp} is calculated as 16.14, 18.45, and 11.53 kcal/mol for α-, β-, and γ-CD, respectively. According to our analysis all CD can make IC with single toluene but the most stable one (with largest E_{comp}) is obtained for β-CD.

In a similar manner, we examine the possibility of two toluene molecules entering the host CD (2 : 1). Initially, two toluene molecules are optimized in vacuum and the equilibrium distance

between them is calculated as 3.6 Å with the interaction energy ($E_{tol\text{-}tol}$) 2.02 kcal/mol which indicates an intermolecular π–π interaction. When toluene pair enters α-CD, it deforms the host and second toluene is expelled as shown in Figure 9(a). Accordingly E_{comp} reduces and becomes 14.90 kcal/mol upon introducing a second toluene when $E_{tol\text{-}tol}$ is taken account indicating that 2 : 1 complex formation is not favored for α-CD. On the other hand, for β-, and γ-CD, toluene pair can fit in the cavity [Figure 9(b,c)] and this further reduces the total energy of the system with increasing E_{comp} to 27.86 and 25.46 kcal/mol, respectively. Finally, our *ab initio* modeling results confirmed 2 : 1 toluene : β-CD stoichiometry and suggests that β-CD cavity is the most suitable host for toluene pair yielding the highest complexation energy.

CONCLUSIONS

In this study, we combined the very high surface area of electrospun nanofibers with the inclusion complexation capability of CD molecules for the efficiently removal of toluene vapor from the surrounding. For this purpose, CD functionalized electrospun nylon 6,6 nanofibrous membranes were produced via electrospinning, using three different types of native CD (α-CD, β-CD, and γ-CD) having 25% and 50% (w/w) weight loading in the nanofiber matrix. SEM images indicated that bead-free nanofibers were obtained by electrospinning of nylon 6,6 and nylon 6,6/CD solutions. The distribution of CD into fiber matrix without forming any crystalline aggregates was confirmed via XRD study. The % weight of CD within resulting nanofibers calculated from TGA thermograms was consistent with the initial CD loading in the solutions used for electrospinning. TGA thermograms of resulting nylon 6,6/CD nanofibers also indicated enhanced thermal stability of both CD and nylon 6,6 owing to the interaction between the polymeric matrix and the CD. ATR-FTIR and XPS analyses indicated that some of CD were located on the surface of nylon 6,6/CD nanofibers. The existence of CD amounts on the fiber surface increased as the CD content increased from 25 thru 50% (w/w, with respect to polymer) in the nylon 6,6/CD nanofibers. Moreover, ATR-FTIR peak shift was observed due to interaction (possibly H bonding) between CD and nylon 6,6. Toluene vapor was used as a model VOC for entrapment experiments. We observed that nylon 6,6/CD nanofibrous membranes entrapped higher amount of toluene when compared to pristine nylon 6,6 nanofibers due to the IC formation capability of the surface associated CD molecules. The entrapment efficiency of toluene vapor was found to be better for nylon 6,6/β-CD nanofibers when compared to nylon 6,6/α-CD and nylon 6,6/γ-CD nanofibers possibly due to better fit and size match between β-CD cavity and toluene. Moreover, our computational modeling results based on first-principles calculations show that, the complexation energy of toluene-CD is higher for β-CD compared to α-CD and γ-CD. Both experimentally and theoretically, β-CD cavity is found the most suitable host for toluene molecule. Our results suggested VOC compounds such as toluene can be removed from the environment using electrospun nylon 6,6 nanofibers functionalized with CD.

ACKNOWLEDGMENTS

Dr. T. Uyar acknowledges TUBITAK-The Scientific and Technological Research Council of Turkey (project #110M612) and EU FP7-PEOPLE-2009-RG Marie Curie-IRG (NANOWEB, PIRG06-GA-2009–256428), and The Turkish Academy of Sciences—Outstanding Young Scientists Award Program (TUBA-GEBIP) for funding the research. F. Kayaci acknowledges TUBITAK-BIDEB (grant #2211) for the national Ph.D. study scholarship. The computational resources have been provided by TUBITAK ULAKBIM, High Performance and Grid Computing Center (TR-Grid e-Infrastructure).

REFERENCES

1. Khin, M. M.; Nair, A. S.; Babu, V. J.; Murugan, R.; Ramakrishna, S. *Energy Environ. Sci.* **2012**, *5*, 8075.
2. Homaeigohar, S.; Elbahri, M. *Materials* **2014**, *7*, 1017.
3. Mo, J.; Zhang, Y.; Xu, Q.; Lamson, J. J.; Zhao, R. *Atmos. Environ.* **2009**, *43*, 2229.
4. World Health Organization, **1989**. "Indoor air quality: organic pollutants." Report on a WHO Meeting, Berlin, 23-27 August 1987. EURO Reports and Studies 111. Copenhagen, World Health Organization Regional Office for Europe.
5. Wang, S.; Ang, H.; Tade, M. O. *Environ. Int.* **2007**, *33*, 694.
6. Kim, Y. M.; Harrad, S.; Harrison, R. M. *Environ. Sci. Technol.* **2001**, *35*, 997.
7. Scholten, E.; Bromberg, L.; Rutledge, G. C.; Hatton, T. A. *ACS Appl. Mater. Interfaces* **2011**, *3*, 3902.
8. Patanaik, A.; Jacobs, V.; Anandjiwala, R. D. *J. Membr. Sci.* **2010**, *352*, 136.
9. Balamurugan, R.; Sundarrajan, S.; Ramakrishna, S. *Membranes* **2011**, *1*, 232.
10. Barhate, R.; Loong, C. K.; Ramakrishna, S. *J. Membr. Sci.* **2006**, *283*, 209.
11. Thavasi, V.; Singh, G.; Ramakrishna, S. *Energy Environ. Sci.* **2008**, *1*, 205.
12. Gopal, R.; Kaur, S.; Feng, C. Y.; Chan, C.; Ramakrishna, S.; Tabe, S.; Matsuura, T. *J. Membr. Sci.* **2007**, *289*, 210.
13. Podgórski, A.; Bałazy, A.; Gradoń, L. *Chem. Eng. Sci.* **2006**, *61*, 6804.
14. Ahn, Y.; Park, S.; Kim, G.; Hwang, Y.; Lee, C.; Shin, H.; Lee, J. *Curr. Appl. Phys.* **2006**, *6*, 1030.
15. Matsumoto, H.; Tanioka, A. *Membranes* **2011**, *1*, 249.
16. Ramaseshan, R.; Sundarrajan, S.; Liu, Y.; Barhate, R.; Lala, N. L.; Ramakrishna, S. *Nanotechnology* **2006**, *17*, 2947.
17. Sundarrajan, S.; Ramakrishna, S. *J. Mater. Sci.* **2007**, *42*, 8400.
18. Kim, H. J.; Pant, H. R.; Choi, N. J.; Kim, C. S. *Chem. Eng. J.* **2013**, *230*, 244.
19. Dasari, A.; Quirós, J.; Herrero, B.; Boltes, K.; García-Calvo, E.; Rosal, R. *J. Membr. Sci.* **2012**, *405*, 134.
20. Roso, M.; Sundarrajan, S.; Pliszka, D.; Ramakrishna, S.; Modesti, M. *Nanotechnology* **2008**, *19*, 285707.
21. Celebioglu, A.; Demirci, S.; Uyar, T. *Appl. Surf. Sci.* **2014**, *305*, 581.
22. Kayaci, F.; Aytac, Z.; Uyar, T. *J. Hazard. Mater.* **2013**, *261*, 286.
23. Crini, G.; Morcellet, M. *J. Sep. Sci.* **2002**, *25*, 789.
24. Szejtli, J. *Water Res.* **1988**, *22*, 1345.

25. Szente, L.; Fenyvesi, É.; Szejtli, J. *Environ. Sci. Technol.* **1999**, *33*, 4495.
26. Uyar, T.; Hunt, M. A.; Gracz, H. S.; Tonelli, A. E. *Cryst. Growth Des.* **2006**, *6*, 1113.
27. Badr, T.; Hanna, K.; De Brauer, C. *J. Hazard. Mater.* **2004**, *112*, 215.
28. Yudiarto, A.; Kashiwabara, S.; Tashiro, Y.; Kokugan, T. *Sep. Purif. Technol.* **2001**, *24*, 243.
29. Del Valle, E. M. *Process Biochem.* **2004**, *39*, 1033.
30. Szejtli, J. *Chem. Rev.* **1998**, *98*, 1743.
31. Hedges, A. R. *Chem. Rev.* **1998**, *98*, 2035.
32. Rekharsky, M. V.; Inoue, Y. *Chem. Rev.* **1998**, *98*, 1875.
33. Connors, K. A. *Chem. Rev.* **1997**, *97*, 1325.
34. Kayaci, F.; Uyar, T. *Polym. Eng. Sci.* **2014**, *54*, 2970.
35. Uyar, T.; Havelund, R.; Nur, Y.; Balan, A.; Hacaloglu, J.; Toppare, L.; Besenbacher, F.; Kingshott, P. *J. Membr. Sci.* **2010**, *365*, 409.
36. Uyar, T.; Havelund, R.; Hacaloglu, J.; Besenbacher, F.; Kingshott, P. *ACS Nano* **2010**, *4*, 5121.
37. Uyar, T.; Havelund, R.; Nur, Y.; Hacaloglu, J.; Besenbacher, F.; Kingshott, P. *J. Membr. Sci.* **2009**, *332*, 129.
38. Heikkilä, P.; Taipale, A.; Lehtimäki, M.; Harlin, A. *Polym. Eng. Sci.* **2008**, *48*, 1168.
39. Huang, L.; McCutcheon, J. R. *J. Membr. Sci.* **2014**, *457*, 162.
40. Kayaci, F.; Ozgit-Akgun, C.; Donmez, I.; Biyikli, N.; Uyar, T. *ACS Appl. Mater. Interfaces* **2012**, *4*, 6185.
41. Manor, P. C.; Saenger, W. *J. Am. Chem. Soc.* **1974**, *96*, 3630.
42. Puliti, R.; Mattia, C. A.; Paduano, L. *Carbohydr. Res.* **1998**, *310*, 1.
43. Lindner, K.; Saenger, W. *Carbohydr. Res.* **1982**, *99*, 103.
44. Harata, K. *Structure* **1987**, *60*, 2763.
45. Kohn, W.; Sham, L. *J. Phys. Rev.* **1965**, *140*, A1133.
46. Hohenberg, P.; Kohn, W. *Phys. Rev.* **1964**, *136*, B864.
47. Kresse, G.; Furthmüller, J. *Phys. Rev. B* **1996**, *54*, 11169.
48. Kresse, G.; Furthmüller, J. *Comput. Mater. Sci.* **1996**, *6*, 15.
49. Allen, F. H. *Acta Crystallogr. Sect. B* **2002**, *58*, 380.
50. Perdew, J. P.; Chevary, J.; Vosko, S.; Jackson, K. A.; Pederson, M. R.; Singh, D.; Fiolhais, C. *Phys. Rev. B* **1992**, *46*, 6671.
51. Grimme, S. *J. Comput. Chem.* **2006**, *27*, 1787.
52. Blöchl, P. E. *Phys. Rev. B* **1994**, *50*, 17953.
53. Ramakrishna, S.; Fujihara, K.; Teo, W.-E.; Lim, T.-C.; Ma, Z. An Introduction to Electrospinning and Nanofibers; World Scientific: Singapore, **2005**.
54. Wendorff, J. H.; Agarwal, S.; Greiner, A. Electrospinning: Materials, Processing, and Applications; Wiley: Germany, **2012**.
55. Uyar, T.; Besenbacher, F. *Polymer* **2008**, *49*, 5336.
56. Uyar, T.; Balan, A.; Toppare, L.; Besenbacher, F. *Polymer* **2009**, *50*, 475.
57. Rusa, C. C.; Bullions, T. A.; Fox, J.; Porbeni, F. E.; Wang, X.; Tonelli, A. E. *Langmuir* **2002**, *18*, 10016.
58. Linggawati, A.; Mohammad, A.; Leo, C. *Mater. Chem. Phys.* **2012**, *133*, 110.
59. Leo, C.; Linggawati, A.; Mohammad, A.; Ghazali, Z. *J. Appl. Polym. Sci.* **2011**, *122*, 3339.
60. Chang, H.-H.; Chen, S.-C.; Lin, D.-J.; Cheng, L.-P. *Desalination* **2013**, *313*, 77.
61. Mehrabanian, M.; Nasr-Esfahani, M.; Jafari, M. *Int. J. Polym. Mater.* **2012**, *61*, 558.
62. Murthy, N.; Curran, S.; Aharoni, S.; Minor, H. *Macromolecules* **1991**, *24*, 3215.
63. Sanatgar, R. H.; Borhani, S.; Ravandi, S. A. H.; Gharehaghaji, A. A. *J. Appl. Polym. Sci.* **2012**, *126*, 1112.
64. Giller, C. B.; Chase, D. B.; Rabolt, J. F.; Snively, C. M. *Polymer* **2010**, *51*, 4225.
65. Huang, L.; Allen, E.; Tonelli, A. E. *Polymer* **1999**, *40*, 3211.
66. Wei, M.; Davis, W.; Urban, B.; Song, Y.; Porbeni, F. E.; Wang, X.; White, J. L.; Balik, C. M.; Rusa, C. C.; Fox, J. *Macromolecules* **2002**, *35*, 8039.
67. Wei, M.; Shin, I. D.; Urban, B.; Tonelli, A. E. *J. Polym. Sci. Part B: Polym. Phys.* **2004**, *42*, 1369.
68. Saenger, W.; Jacob, J.; Gessler, K.; Steiner, T.; Hoffmann, D.; Sanbe, H.; Koizumi, K.; Smith, S. M.; Takaha, T. *Chem. Rev.* **1998**, *98*, 1787.
69. Kayaci, F.; Uyar, T. *Carbohydr. Polym.* **2012**, *90*, 558.
70. Kayaci, F.; Uyar, T. *J. Agric. Food Chem.* **2011**, *59*, 11772.
71. Uyar, T.; Havelund, R.; Hacaloglu, J.; Zhou, X.; Besenbacher, F.; Kingshott, P. *Nanotechnology* **2009**, *20*, 125605.
72. Kojima, Y.; Matsuoka, T.; Takahashi, H. *J. Appl. Polym. Sci.* **1999**, *74*, 3254.
73. Sambasevam, K. P.; Mohamad, S.; Sarih, N. M.; Ismail, N. A. *Int. J. Mol. Sci.* **2013**, *14*, 3671.
74. Rusa, C. C.; Uyar, T.; Rusa, M.; Hunt, M. A.; Wang, X.; Tonelli, A. E. *J. Polym. Sci. Part B: Polym. Phys.* **2004**, *42*, 4182.
75. Uyar, T.; Besenbacher, F. *Eur. Polym. J.* **2009**, *45*, 1032.
76. Gardner, S. D.; Singamsetty, C. S. K.; Booth, G. L.; He, G.-R.; Pittman, C. U., Jr. *Carbon* **1995**, *33*, 587.
77. Hariharan, A.; Kumar, S. K.; Russell, T. P. *Macromolecules* **1990**, *23*, 3584.
78. Hunley, M. T.; Harber, A.; Orlicki, J. A.; Rawlett, A. M.; Long, T. E. *Langmuir* **2008**, *24*, 654.
79. Walton, D.; Mayes, A. *Phys. Rev. E* **1996**, *54*, 2811.
80. Walton, D.; Soo, P.; Mayes, A.; Sofia Allgor, S.; Fujii, J.; Griffith, L.; Ankner, J.; Kaiser, H.; Johansson, J.; Smith, G. *Macromolecules* **1997**, *30*, 6947.
81. Chalumot, G.; Yao, C.; Pino, V.; Anderson, J. L. *J. Chromatogr. A* **2009**, *1216*, 5242.
82. Schwartz, A.; Bar, R. *Appl. Environ. Microbiol.* **1995**, *61*, 2727.
83. Chakraborty, M.; Ivanova-Mitseva, P.; Bart, H. *J. Sep. Sci. Technol.* **2006**, *41*, 3539.
84. Kayaci, F.; Ertas, Y.; Uyar, T. *J. Agric. Food Chem.* **2013**, *61*, 8156.
85. Kayaci, F.; Uyar, T. *Food Chem.* **2012**, *133*, 641.
86. Kayaci, F.; Umu, O. C.; Tekinay, T.; Uyar, T. *J. Agric. Food Chem.* **2013**, *61*, 3901.
87. Schneiderman, E.; Stalcup, A. M. *J. Chromatogr. B* **2000**, *745*, 83.